JOURNAL OF SPACECRAFT AND ROCKETS
Vol. 32, No. 3, May–June 1995

Wing-Body Carryover for Noncircular Missiles

Brian E. Est* and H. F. Nelson†
University of Missouri—Rolla, Rolla, Missouri 65401

$K_{W(B)}$, the wing-body carryover factor due to body upwash on an undeflected wing, and wing center of pressure (CP) are investigated for unbanked, supersonic missiles with square and triangular fuselage cross sections at low angles of attack. The parametric effects of Mach number, wing leading-edge sweep back angle, angle of attack, and body cross-sectional shape on $K_{W(B)}$ and wing CP were numerically examined. The calculations were performed using a spatial marching Euler code ZEUS. Predicted $K_{W(B)}$ results were compared to slender-body theory values historically used for preliminary missile design. Computed $K_{W(B)}$ and wing CP results were found to exhibit sensitivity to Mach number, wing leading-edge sweep angle, and body cross-sectional shape. Euler $K_{W(B)}$ and wing CP values generally compare favorably to slender-body theory predictions in trend, but differ in magnitude by up to 15%. ZEUS predictions of $k_{W(B)}$, the wing-body interference factor for an all-moving control surface, are also presented for square fuselage cross sections. All computed results are valid for missiles in the "+" orientation at small angles of attack and Mach numbers from 2 to 4. Data are presented to extend the missile preliminary design data base for arbitrary cross-sectional bodies.

Nomenclature

A = coefficient reference area (circular base area), cm^2
a = shape factor (see Appendix)
C_N = normal force coefficient
C_{N_α} = normal force coefficient slope with angle of attack, deg^{-1}
C_{N_δ} = normal force coefficient slope with all-moving control deflection angle, deg^{-1}
C_P = pressure coefficient
$K_{W(B)}$ = wing-body carryover factor due to body upwash, $\delta =$ 0 deg
$k_{W(B)}$ = wing-body interference factor due to control deflection, $\alpha = 0$ deg
M = freestream Mach number
R = radius of inscribed circle in the forebody base, cm
r = radial direction from the body centerline
S = wing semispan from fuselage centerline, cm
V = freestream velocity
V_c = crossflow velocity, $V \sin\alpha$
V_{NW} = component of crossflow velocity normal to wing
V_t = component of crossflow velocity tangent at body surface
Y' = dimensionless distance from the body centerline, y/R
y = lateral distance from longitudinal missile axis, cm
Z = axial distance from nose tip, cm
Z' = dimensionless axial distance behind leading edge of wing $(Z - Z_{LE})/R$
α = angle of attack, deg
δ = control deflection angle of all-moving wing, deg
θ = angle between V_t and V_{NW} in crossflow plane, deg
Λ = wing leading-edge sweep angle, deg
ϕ = aerodynamic roll angle or angular direction in crossflow plane, deg

Subscripts

hinge = axial location of wing hinge
LE = wing leading edge at root chord
TE = wing trailing edge at root chord
v = due to vortices
W = wing alone
$W(B)$ = wing in the presence of the body

Received July 26, 1991; revision received March 3, 1993; accepted for publication April 12, 1993.

*Graduate Student, Department of Mechanical and Aerospace Engineering and Engineering Mechanics; currently Aerospace Engineer, Dynetics, Inc., Flight Vehicle Analysis Branch, 1000 Explorer Blvd., Huntsville, AL 35814-5050. Member AIAA.

†Professor Aerospace Engineering, Thermal Radiative Transfer Group. Associate Fellow AIAA.

Introduction

CONVENTIONAL tactical missiles, launched from platforms using rail, rotary, armored box, or tube launchers, are usually circular in body cross section. Rail launchers use an external carriage mechanism and usually do not impose geometric constraints on missile body cross sections. Tube, armored box, and rotary launchers store missiles internally prior to launch, and therefore have distinct geometric packaging requirements. The cross-sectional shape of tube launchers is usually circular, but rotary and armored box launchers can be triangular and square, respectively.

Conventional missiles with circular fuselage cross sections packaged in noncircular launch containers do not efficiently use the launcher volume. A missile with a body cross section similar to the launch container would have more internal volume available for a larger warhead, greater fuel storage capacity, electronics, or submunitions. Previous research has shown that noncircular body-alone configurations exhibit higher normal force and lift-to-drag ratios than circular bodies,[1–6] especially for shapes with flat windward faces. These packaging and performance attributes are attractive and have lead to interest in missiles with noncircular fuselage cross sections. In the present research, missiles with noncircular fuselage cross sections are investigated to determine if noncircular body cross sections can yield potentially improved aerodynamics for wing-body configurations.

The conceptual and preliminary stages of tactical missile design are characterized by frequent design modifications and constraints on both cost and time. Therefore, rapid, engineering-level prediction techniques, such as component buildup methods, are utilized by missile designers. Component buildup methods consider the individual components of the configuration and account for the nonlinear interaction between components to synthesize the total configuration aerodynamics. These methods have demonstrated accuracy suitable for conceptual and preliminary design.[7] The component buildup method of NACA Rept. 1307 (Ref. 8) has historically been the foundation to which additional modeling improvements have been made, e.g., the equivalent angle-of-attack method.[9–14] These component buildup methods use slender-body theory[15] to compute values of the nonlinear wing-body carryover and interference factors, $K_{W(B)}$ and $k_{W(B)}$.

The equivalent angle-of-attack component buildup method combines the effects of wing-body carryover and flowfield vortices to

compute an equivalent angle of attack for the component in the presence of the body. The normal force coefficient on a missile wing at low angle of attack is

$$C_{N_{W(B)}} = [K_{W(B)}\alpha + k_{W(B)}\delta + (\Delta\alpha)_v](C_{N_\alpha})_W \quad (1)$$

where the equivalent angle of attack is defined as

$$\alpha_{eq} = K_{W(B)}\alpha + k_{W(B)}\delta + (\Delta\alpha)_v \quad (2)$$

$K_{W(B)}$, $k_{W(B)}$, and $(\Delta\alpha)_v$ correspond to wing-body carryover due to the body upwash on the undeflected wing, interference due to all-moving wing deflection, and vortex effects, respectively. The component of equivalent angle of attack for wing-body carryover due to body upwash for an undeflected wing is defined as

$$K_{W(B)} = (C_{N_\alpha})_{W(B)}/(C_{N_\alpha})_W, \qquad \delta = 0, \quad \alpha \geq 0 \quad (3)$$

A similar wing-body interference factor is defined in the equivalent angle-of-attack method for the interference effect of a control deflection, and is given by

$$k_{W(B)} = (C_{N_\delta})_{W(B)}/(C_{N_\alpha})_W, \qquad |\delta| \geq 0, \quad \alpha = 0 \quad (4)$$

where δ is essentially the wing angle of attack. The wing is assumed to be an all-moving delta wing. In this research, the hinge located at the planform geometric centroid

$$Z_{hinge} = \tfrac{2}{3}(Z_{TE} - Z_{LE}) + Z_{LE} \quad (5)$$

Favorable carryover ($K_{W(B)} > 1$) can nearly double the wing equivalent angle of attack; therefore, carryover factors are considered significant parameters to the missile designer.

Force and moment data bases exist for wing-alone and body-alone missile components; therefore, the purpose of this research is to develop a data base for component buildup parameters for noncircular bodies suitable for conceptual and preliminary design. Mach number, body cross-sectional shape, wing leading-edge sweep angle, wing deflection angle (for square cross sections only), and angle of attack are parametrically varied to develop a matrix of $K_{W(B)}$, $k_{W(B)}$, and wing CP values. These data are valid for supersonic, unbanked, body-wing missiles with circular, square, diamond, triangular, and inverted-triangular fuselage cross sections oriented in the "+" configuration.

Analytical Methodology

Governing Equations

The steady, three-dimensional Euler equations are utilized for this research due to their computational efficiency and accuracy for supersonic missile configurations. The pressure distribution given by the Euler equations is accurate for attached flow and can be integrated over the entire body to yield inviscid forces and moments. The Euler equations have been shown to give accurate results for missile configuration aerodynamics.[1,16–18] A spatial marching Euler code ZEUS is used for this research. ZEUS[19–21] uses a finite volume formulation of the steady, three-dimensional Euler equations based on the upwind Godunov scheme,[22,23] providing second-order accuracy.

The Euler equations convect vorticity and determine the circulation generated by shocks, but viscous phenomena, such as vortex shedding from smooth body surfaces, must be empirically modeled. Instead of flow separating and rolling up to form leeside-vortices, inviscid calculations feature crossflow shocks that may generate sufficient vorticity to form leeside vortices. At moderate to large angles of attack, the computed vortex strength is much smaller than experimental measurements. The computed vortex pressure distributions differ from measured distributions; however, at small angles of attack ($\alpha < 6$ deg) this difference is usually small.

At angles of attack greater than about 4 deg, viscous crossflow about a circular missile body will begin to separate and roll up to form leeside vortices. For missiles with noncircular fuselage cross sections, the corners of the noncircular cross-sectional shapes produce vortices which cause nonlinear aerodynamic effects. Work exists that shows that, at low angles of attack ($\alpha \leq 5$ deg), viscous effects are not substantial. Jorgensen[5] performed wind tunnel flow visualization investigations of forebodies with noncircular cross sections at Mach 1.98 and 3.88. Square and triangular body cross-sectional shapes with shape factors a of 0.9748 and 0.9834 (see the Appendix), respectively, were examined at angles of attack ranging from 0 to 17 deg. At moderate angles of attack, the corners of the noncircular cross sections produced strong leeside vortex systems. Leeside vortices were most prevalent at angles of attack greater than 5 deg. Est and Nelson[18] compared ZEUS predictions of noncircular missile forebody lift with wind tunnel data from Carlson and Gapcynski[4] for 0 deg $\leq \alpha \leq$ 6 deg. Their results showed good agreement for lift coefficient at Mach number = 2.01 and $a = 0.5580$ and 0.5122 for square and triangular fuselage cross sections, respectively. The cross-sectional shapes examined in the present research have shape factors of $a \leq 0.75$. The angle of attack range for the calculations is $\alpha \leq 5$ deg; therefore, viscous effects should be small and the Euler equations should accurately model the flowfield.

Cross-Sectional Shape and Wing Position

Figure 1 illustrates wing position and nomenclature. Carryover factors are computed for the horizontal wings. For square, circular, and diamond fuselage cross sections, the wings are located symmetrically on the fuselage. For triangular and inverted-triangular fuselage cross sections, horizontal wings are located in the horizontal plane through the equilateral corners, and vertical wings pass through the body centerline. The selection of the baseline wing positions was driven by the requirement that the wings be folded while the missile is stored in the launcher.

All fuselage cross-sectional shapes investigated are related by a common shape factor a. A derivation and illustration of the shape factor are included in the Appendix. The shape factor varies from 0 to 1 and it quantifies the fuselage cross-sectional shape. When $a = 0$, all shapes become circular in cross section with common radius R. When $a = 1$, the cross-sectional shapes become sharp-cornered squares or triangles, depending upon the shape of interest.

All the fuselage cross-sectional shapes are developed around a circular cross section of radius R; consequently, the location of the wing root chord position (y/R) is a function of shape factor a. This implies that changing the cross-sectional shape of the fuselage (changing a) shifts the position of the wing root chord relative to the fuselage centerline, resulting in different, shifted values of S/R.

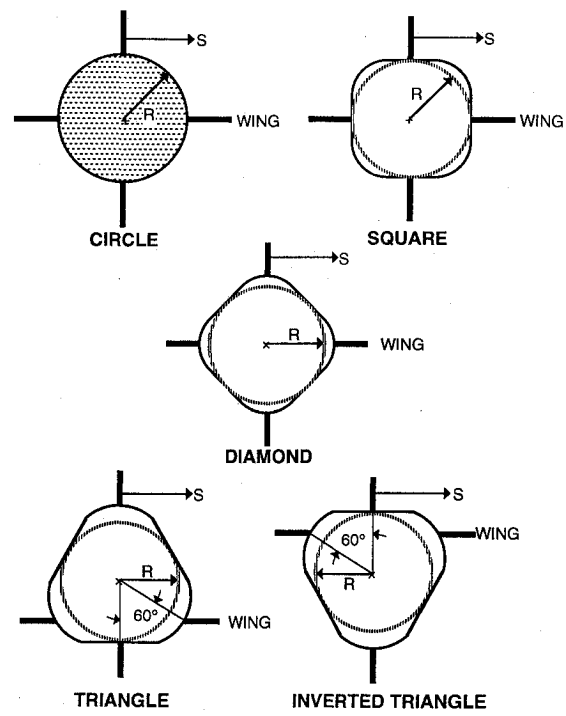

Fig. 1 Fuselage cross-sectional shapes and baseline wing positions.

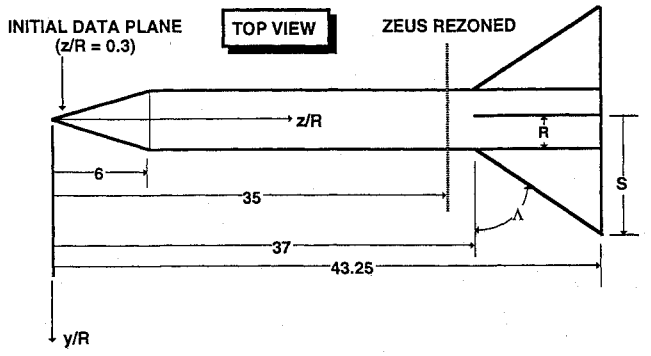

Fig. 2 Missile geometry.

Thus, for triangular, diamond, and inverted-triangular fuselage cross sections, the wing root chord is not located at $y/R = 1$, e.g., it is at $y/R = 1.299$ for a wing on an $a = 0.5$ triangular fuselage cross section (see Fig. 1). For data comparison purposes, it was not practical to account for this shift. The position $S/R = 1$ is always located at the wing root chord independent of the body cross section, and the position $S/R = 6$ implies a wing with a span that extends outward five body radii ($5R$) from the wing root chord position.

Missile Configuration

Figure 2 illustrates a dimensioned line drawing of the missile geometry used in this research. The nosecone is linearly tapered in cross section from a circle at $Z/R = 0.3$ to the cross-sectional shape of interest at $Z/R = 6$. For $Z \geq 6$, the fuselage has a constant cross-sectional shape. ZEUS computations begin at an initial data plane located at $Z/R = 0.3$. The conditions on the initial data plane are generated by a one-dimensional conical starting solution that takes the calculations across the bow shock. ZEUS calculations are axially marched down the body using a single zone, 36 × 36, (r by ϕ) grid for the forebody calculations ($0.3 \leq Z/R \leq 35$) at 90% of the maximum axial step marching size for numerical stability, Courant–Friedrichs–Lewy (CFL) step limit. At $Z/R = 35$, the computations are stopped and the code is rezoned for the calculations over the missile wings. ZEUS was configured with two, 36 × 36 zones for $35 \leq Z/R \leq 43.25$ and run at 20% the CFL limit. Reducing the maximum CFL limit reduces the spatial marching step and increases the number of axial grid points on the wings. Pitch plane symmetry is utilized to reduce computer storage and run time. Mesh clustering was not used. All of the ZEUS computations were made using the IBM 4381 computer at the University of Missouri–Rolla. CPU times ranged from about 60 to 100 min for complete missile flowfield solutions.

Wing-Alone Lift

The missile delta wings used in this research are zero-thickness lifting surfaces with a leading-edge sweep back angle, Λ. The planar wings are oriented in the "+" configuration. Lifting surface theory[15] is used to determine the wing-alone normal force curve slope. The normal force curve slope is given as

$$(C_{N_\alpha})_W = \frac{4}{\sqrt{M^2 - 1}} \tag{6}$$

This theory is valid for supersonic leading edges and attached flow.

Small S/R Considerations

At $S/R < 2$, the Euler predictions of $(C_{N_\alpha})_{W(B)}$ become inaccurate due to the small number of grid points resolving the flowfield on the wing. Another method was required to supplement ZEUS small $(S/R)(C_{N_\alpha})_{W(B)}$ predictions and to provide $K_{W(B)}$ values for the limit as S/R approaches 1. Note that as S/R approaches 1, the missile becomes a fuselage without wings.

At angle of attack, the fuselage is essentially a two-dimensional cylinder in the plane of the crossflow velocity, as illustrated in Fig. 3. The limiting values of $K_{W(B)}$ as S/R approaches 1 can be calculated from the crossflow velocity distribution over the fuselage. Reference 24 provides pressure coefficient data for the fuselage cross-sectional shapes investigated in this research. The analytical data were computed using a conformal mapping transformation of the noncircular cylinder into a circular cylinder in the complex potential plane. For incompressible flow, velocity is related to pressure coefficient by

$$V_t = V \sin\alpha\sqrt{1 - C_P} = V_c\sqrt{1 - C_P} \tag{7}$$

The crossflow velocity data are related to $K_{W(B)}$ in the limit as S/R approaches 1 by

$$K_{W(B)} = V_{NW}/V_c = V_t \cos\theta/V_c \tag{8}$$

From Eqs. (7) and (8),

$$K_{W(B)} = \cos\theta\sqrt{1 - C_P} \tag{9}$$

$S/R = 1$ implies that the wing span is infinitesimally small; therefore, the wing-body carryover becomes proportional to the crossflow velocity at the body surface. The Euler computations should approach the potential flow solutions at the body surface; therefore, the ZEUS solutions presented are faired from approximately $S/R = 2$ to $S/R = 1$ to match the limiting potential flow solutions of $K_{W(B)}$ at $S/R = 1$ given in Table 1.

Data were available from Ref. 24 for the circular cross-sectional shape ($a = 0$) and at $a = 0.60$ and 0.65 for the square and triangular cross sections, respectively. These data were linearly interpolated in a to determine $K_{W(B)}$ at $S/R = 1$ for the shape factor of interest. The results are given in Table 1.

Table 1 Potential flow values of $K_{W(B)}$ as S/R approaches 1

Cross-sectional shape	Shape parameter, a					
	0.00	0.25	0.50	0.60	0.65	0.75
Square	2.00	1.77	1.53	1.50	—	1.30
Diamond	2.00	2.05	2.10	2.12	—	2.15
Triangle	1.50[a]	1.59	1.68	—	1.73	1.77
Inverted triangle	1.50[a]	1.59	1.68	—	1.73	1.77

[a]Wing vertical position is above the missile centerline for these circular bodies (ϕ = 60 deg, see Fig. 3).

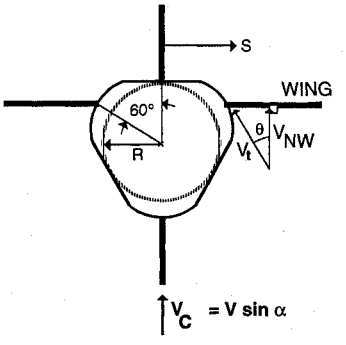

Fig. 3 Crossflow velocity vector diagram used to determine limit of $K_{W(B)}$ as S/R approaches 1.

Results and Discussion

Flight Conditions

Nominal flight conditions and wing geometry for this research are $M = 3$, $\alpha = 3$ deg, and $\Lambda = 51.34$ deg. Table 2 presents the matrix of flight conditions and geometries used in the analysis of $K_{W(B)}$ and wing CP for the square, diamond, triangular, and inverted-triangular fuselage cross sections. Recall that when $a = 0$, all of the cross sections are circular.

Flowfield Physics

Figure 4 shows the crossflow velocity field for an $a = 0.75$ inverted-triangular fuselage cross section for wings with a span of $S/R = 4$. The length of the arrows is proportional to the magnitude

Table 2 Flight conditions and geometries

Mach number	α, deg	cot Λ	Shape factor, a
2.0	3.0	0.8	0.00, 0.25, 0.50, 0.75
3.0	1.0	0.8	0.00, 0.25, 0.50, 0.75
3.0	3.0	0.6, 0.8, 1.0	0.00, 0.25, 0.50, 0.75
3.0	5.0	0.8	0.00, 0.25, 0.50, 0.75
4.0	3.0	0.8	0.00, 0.25, 0.50, 0.75

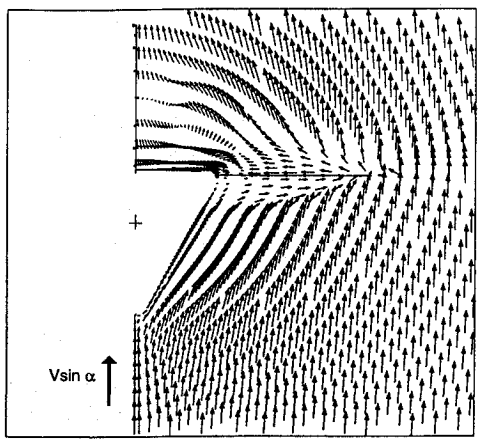

Fig. 4 Crossflow velocity vectors for an inverted triangular cross section: $a = 0.75$, $M = 4.0$, $\alpha = 3$ deg, $S/R = 4.0$, $\Lambda = 51.34$ deg, and $\delta = 0$ deg.

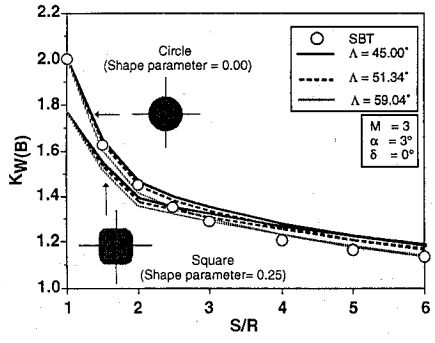

Fig. 5 Effect of wing leading-edge sweep back angle on $K_{W(B)}$ for missiles with square and circular cross sections.

$S/R = 4$. The length of the arrows is proportional to the magnitude of the crossflow velocity and the arrows point in the direction of the velocity vector. It shows the expansion and shock waves above and below the wing, respectively. This flowfield is complex with a large vortex visible above the leeward side of the body. This large vortex was only evident on the triangular shapes at $a = 0.75$.

Wing Leading-Edge Sweep Back Angle Effects

Figure 5 shows $K_{W(B)}$ as a function of wing span for three wing leading-edge sweep back angles for both circular and square fuselage cross sections. The values of $K_{W(B)}$ from slender-body theory (SBT) are shown as the circular symbols. As Λ decreases from 59.04 deg (cot $\Lambda = 0.6$) to 45.00 deg (cot $\Lambda = 1.0$), $K_{W(B)}$ slightly increases throughout the range of S/R. This trend is consistent for all cross-sectional shapes investigated. Slender body theory predictions of $K_{W(B)}$ agree well in magnitude and trend with the circular cross section calculations for $1 \leq S/R \leq 6$, but are larger in magnitude than the square fuselage cross section $K_{W(B)}$ values for $S/R < 2.5$.

Body Cross-Sectional Shape Effects

Figures 6 and 7 illustrate the effect of increasing shape factor on $K_{W(B)}$ as a function of S/R for wings on inverted-triangular and triangular, and square and diamond fuselage cross sections, respectively. In Fig. 6, the $a = 0.75$ data have been curve fit to the potential flow solutions $S/R = 1$ and 2.5 for the triangle and

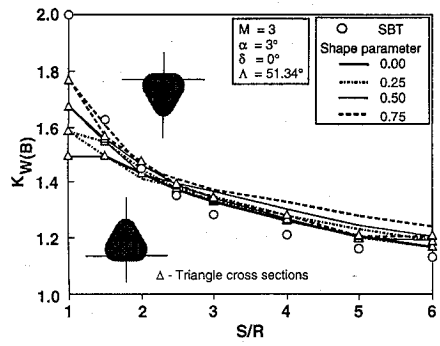

Fig. 6 Effect of a on $K_{W(B)}$ for missiles with triangular and inverted-triangular cross sections.

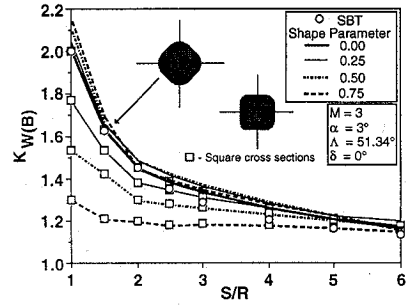

Fig. 7 Shape parameter effects on $K_{W(B)}$ for missiles with diamond and square cross sections.

$S/R = 1$ and 3 for the inverted triangle, respectively. In Fig. 6, $K_{W(B)}$ slightly increases for the entire range of S/R as shape factor increases for the inverted-triangular cross sections.

The $K_{W(B)}$ values for the triangular fuselage cross sections in Fig. 6 show little sensitivity to a as a increases for wings with $S/R > 3.5$. SBT predictions of $K_{W(B)}$ for $S/R > 2$ are close to ZEUS predictions of $K_{W(B)}$ for the triangular fuselage cross section. For $S/R < 3$, the $a = 0$ cases for the triangles and inverted triangles with S/R approaching 1 do not approach the circular-body shape limit of 2.0. This trend is due to the horizontal delta wing location on the shoulder of the triangles above (inverted triangle) and below (triangle) the longitudinal body axis (see Fig. 1 and Table 1). There is $a = 0$ $K_{W(B)}$ data for wings located vertically off the centerline[25] and it agrees with the ZEUS $K_{W(B)}$ values for all S/R.

Figure 7 shows $K_{W(B)}$ as a function of S/R for several shape factors for the square and diamond fuselage cross sections. $K_{W(B)}$ values for the square cross sections decrease as a increases for $S/R \leq 6$. Potential flow solutions are curve fit to ZEUS values for $1 \leq S/R \leq 1.5$. Note that SBT values are markedly higher than the Euler predictions over the entire range of a and S/R for the square cross sections. For $a = 0$ the agreement with SBT is reasonably good, since this corresponds to a circular cross section with the wings on the centerline.

Increasing the shape factor magnitude has little influence on $K_{W(B)}$ throughout the range of S/R for the diamond fuselage cross sections. The diamond cross sections values of $K_{W(B)}$ agree well with SBT-predicted $K_{W(B)}$ values for all S/R. This is due to the similarity between the flowfield in the crossflow plane about the diamond and circle body shapes.

Mach Number Effects

Figures 8 and 9 illustrate the influence of Mach number variation on $K_{W(B)}$ for the five missile fuselage cross-sectional shapes of this research. The trend typical of all fuselage cross sections at any a is that as Mach number increases from 2 to 4, $K_{W(B)}$ increases for all S/R. SBT predictions of $K_{W(B)}$ for circular cross sections generally lie between the $M = 2$ and $M = 3$ curves predicted by ZEUS. This implies that as Mach number increases above 3, values of $K_{W(B)}$ can become considerably larger than SBT predictions for low angles of attack.

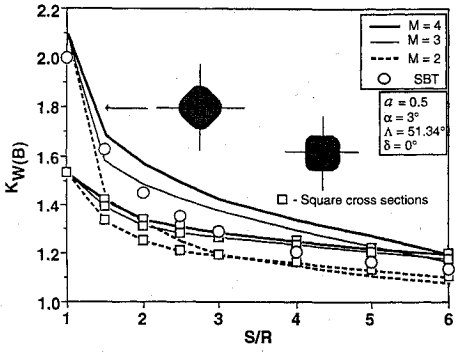

Fig. 8 Mach number effects on $K_{W(B)}$ for diamond and square cross sections.

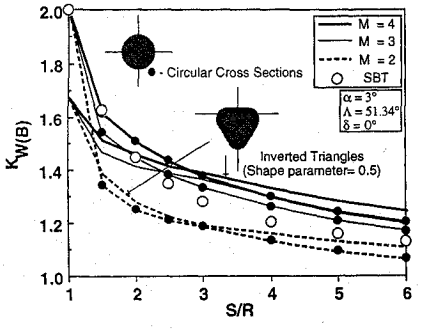

Fig. 9 Effect of increasing Mach number on $K_{W(B)}$ for inverted-triangular and circular cross sections.

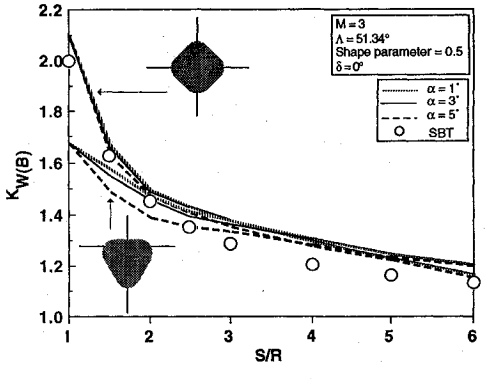

Fig. 10 Effect of increasing angle of attack on $K_{W(B)}$ for diamond and inverted-triangular cross sections.

Angle-of-Attack Effects

If the slope of the wing normal force is linear with angle of attack, $K_{W(B)}$ values should not vary with changes in angle of attack. Figure 10 illustrates that the range of flight conditions in this research occur in the linear range of angle of attack. It shows $K_{W(B)}$ values vs S/R for the diamond and inverted-triangular fuselage cross sections for $\alpha = 1$, 3, and 5 deg. This research is predicated on the assumption that the flight conditions are in the linear range of angle of attack (lifting-surface theory), and that any nonlinearities are due to flight parameters other than angle of attack. Figure 10 shows that $K_{W(B)}$, for the inverted-triangular and diamond fuselage cross sections, is not appreciably affected by angle of attack for $\alpha < 5$ deg.

Wing Center of Pressure

Figures 11 through 15 show the loci of center of pressure as functions of Λ, M, a, and S/R for all the various fuselage cross section shapes. The ordinate of the figures is $Y' = y/R$. The abscissa of the figures is the axial distance from the leading edge of the wing root chord divided by R. The symbols along the curves represent specific values of S/R.

The effect of changing the wing leading-edge sweep back angle on wing center of pressure is presented in Fig. 11 for triangular and circular fuselage cross sections. As Λ decreases from 59.04 to 45.00 deg, the wing CP moves forward and slightly inboard. This trend is evident for all cross-sectional shapes and for all S/R values. Note that the wing CP is always located near the geometric centroid of the wing planform.

Figure 12 shows the effect of increasing shape factor on wing CP for diamond fuselage cross sections. Since the wings are located on the corner of the fuselage, the wing root chord moves outboard as a increases. Thus all the curves are parallel with the

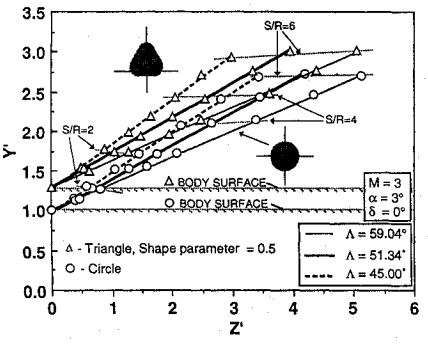

Fig. 11 Leading-edge sweep back angle effects on wing CP for triangle and circle cross sections for S/R = 1.5, 2.0, 2.5, 3.0, 4.5, and 6.0.

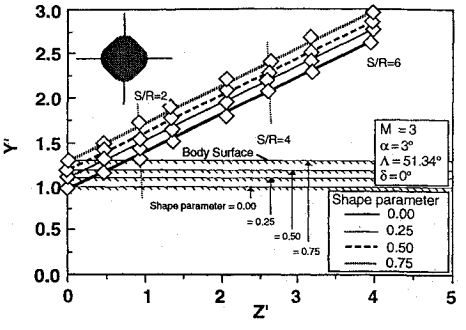

Fig. 12 Shape parameter effects on wing CP for diamond cross sections for S/R = 1.5, 2.0, 2.5, 3.0, 4.5, and 6.0.

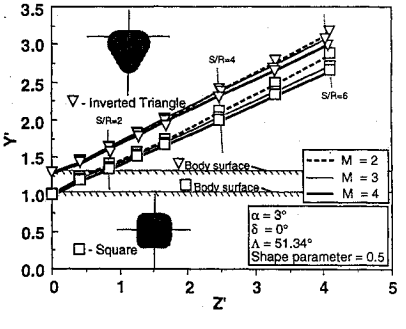

Fig. 13 Mach number effects on wing CP for inverted-triangular and square cross sections for S/R = 1.5, 2.0, 2.5, 3.0, 4.5, and 6.0.

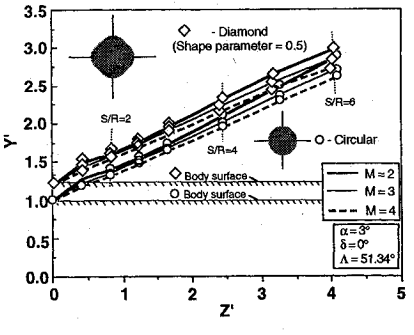

Fig. 14 Mach number effects on wing CP for diamond and circular cross sections for S/R = 1.5, 2.0, 2.5, 3.0, 4.5, and 6.0.

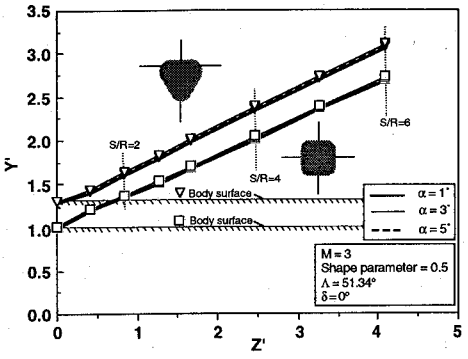

Fig. 15 Angle-of-attack effects on wing CP for square and inverted-triangular cross sections for S/R = 1.5, 2.0, 2.5, 3.0, 4.5, and 6.0.

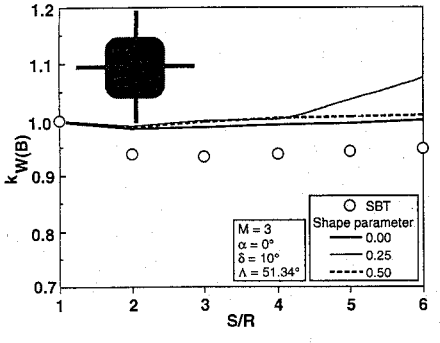

Fig. 16 Shape parameter effects on $k_{W(B)}$ for square and circular cross sections.

displacement being directly proportional to a. The trend of outboard displacement occurs for the triangular and inverted-triangular fuselage cross sections, but not for the square fuselage cross sections because for these shapes changing a does not move the root chord.

Wing CP for all of the cross-sectional shapes moves inboard as the Mach number is increased. This is illustrated in Figs. 13 and 14 for the inverted-triangular and square fuselage cross sections, and the diamond and circular fuselage cross sections, respectively. The wing CP is a measure of the distribution of the pressure on the surface of the missile wing. The wing CP moves inboard because as the Mach number increases, the crossflow velocity (upwash) increases. The upwash is largest at the wing root chord ($y/R = 1$) and decreases as y/R increases. An increase in upwash results in an increase in pressure near the wing root chord, thereby moving the wing CP inboard.

Figure 15 presents the effect of changing angle of attack on wing CP for triangular and square fuselage cross sections. The wing CP is not affected by increasing in the angle of attack from 1 to 5 deg, because the wing forces and movements are linear in angle of attack.

Wing Control Deflection

The wing-body interference factor for all-moving controls is given by $k_{W(B)}$. The effect of increasing shape factor on $k_{W(B)}$ is shown in Fig. 16 for square and circular fuselage cross sections for an all-moving wing deflection of 10 deg, as a function of S/R. ZEUS $k_{W(B)}$ values and SBT values differ by less than 10% for the entire range of S/R for the $a = 0$ and $a = 0.5$ fuselage cross sections, and for $S/R < 4$ for the $a = 0.25$ square fuselage cross sections. At $S/R = 4$, the $k_{W(B)}$ data for an $a = 0.25$ square fuselage cross section break away from SBT, the $a = 0$, and $a = 0.5$ cases. The $a = 0$ and 0.25 fuselage cross sections both have gaps between the wing root chord and the fuselage when $\delta = 10$ deg. For the $a = 0.25$ fuselage cross section, the gap begins for wings whole root chords correspond to a span of $S/R \sim 4$; the circular ($a = 0$) fuselage cross section has gaps for all wing deflections. The reason that $k_{W(B)}$ for the $a = 0.25$ fuselage cross section breaks away from the SBT and $a = 0$ fuselage data for $k_{W(B)}$ is not fully understood at this time and merits further investigation. It may be due to a larger gap at the leading edge than at the trailing edge due to the hinge displacement or porting effects. Wing CP was not otherwise appreciably affected by increasing shape factor for the deflected wing cases.

All of the preceding $K_{W(B)}$, $k_{W(B)}$, and wing CP data have been tabulated in Ref. 1 for use in the conceptual and preliminary design analysis of arbitrary cross section missile bodies. Curve fits of the tabulated $K_{W(B)}$ and wing CP results of Ref. 1 can be easily incorporated into an aeroprediction code such as Missile Datcom for rapid synthesis of arbitrary body configuration aerodynamics.

Conclusions

A spatial marching Euler code, ZEUS, has been used to determine the effect of Mach number M, wing leading-edge sweep back angle Λ, fuselage cross-sectional shape a, and angle of attack α on $K_{W(B)}$ and wing center of pressure (CP) for supersonic body-wing missiles with noncircular fuselage cross sections. Values of $K_{W(B)}$ and wing CP were determined for wing spans of $1 \leq S/R \leq 6$ on bodies with square, diamond, circular, triangular, and inverted-triangular fuselage cross sections. The $K_{W(B)}$ values computed by ZEUS were compared to slender-body theory (SBT) predictions. SBT values of carryover factors are presently used in engineering-level aerodynamic prediction codes. The values are a function only of S/R. Euler $K_{W(B)}$ values have been shown to be sensitive to M, Λ, and a in addition to S/R, although never differing by more than 15% from SBT predictions.

$K_{W(B)}$ values always substantially increase with increasing Mach number (2–4) and always slightly increase with decreasing leading-edge sweep back angle (59.04–45.00 deg). As body cross-sectional shape became increasingly noncircular ($a > 0$), $K_{W(B)}$ values for the square bodies markedly decrease, but remain essentially unchanged for the triangular, inverted-triangular, and diamond bodies. Changing Mach number, leading-edge sweep back angle, and shape parameter were found to exhibit only a slight effect on wing CP for zero-thickness delta wings in the "+" orientation. Generally, the wing CP is located at or near the geometric centroid of the triangular wing planform.

The effects of body cross-sectional shape on $k_{W(B)}$ were investigated for missiles with square fuselage cross sections and all-moving delta wings. The $k_{W(B)}$ values predicted by ZEUS generally differ with SBT predictions by less than 10%. However, when gaps exist between the square fuselage and the all-moving wing root chord due to wing deflections (large S/R), ZEUS predicted $k_{W(B)}$ values are markedly higher than SBT.

Appendix: Development of the Shape Factor Parameter, a

Parameter a quantifies the body cross-sectional shape of the missile fuselage. At $a = 0$, the shape is circular and at $a = 1$, the shape is sharp-cornered, i.e., a sharp-cornered square. Figure A1 shows the relationship between shape factor and the geometry of the noncircular fuselage cross sections. For the square cross sections, the circular fillet, defined by R_f, is scribed over an arc of 90 deg. For

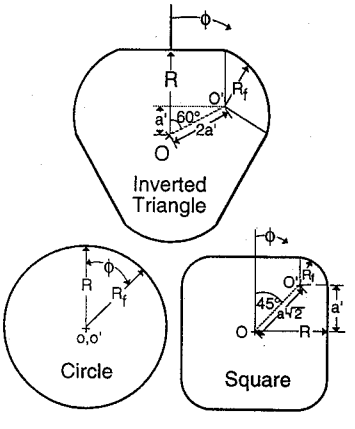

Fig. A1 Shape parameter geometry.

the triangular cross sections, R_f is scribed over a 120 deg arc. For the circular cross section, the fillet scribes a circle.

R_f and a' are defined in term of the radius R of the inscribed circle (Fig. A1)

$$R = R_f + a' \tag{A1}$$

Thus one can write

$$a'/R + R_f/R = 1 \tag{A2}$$

However, the parameter a is defined as a'/R so that

$$a = 1 - R_f/R \tag{A3}$$

As a approaches 0, R_f approaches R and as a approaches 1, R_f approaches 0.

Acknowledgments

This University of Missouri–Rolla work has been supported by McDonnell Douglas Missile Systems Company of St. Louis, Missouri, through the Independent Research and Development Program, monitored by Kurt D. Bausch. Additional funds were provided by the Missouri Research Assistance Act.

References

[1]Est, B. E., "Computational Aerodynamics of Supersonic Missiles with Noncircular Fuselage Cross Section," M. S. Thesis, Dept. of Mechanical and Aerospace Engineering and Engineering Mechanics, Univ. of Missouri–Rolla, MO, May 1991.

[2]Sigal, A., and Lapidot, E., "Aerodynamic Characteristics of Configurations Having Bodies with Square, Rectangular, and Circular Cross-Sections," *Journal of Spacecraft and Rockets*, Vol. 25, No. 2, 1989, pp. 85–89.

[3]Hutt, G. R., and Howe, A. J., "Effects of Cross Section and Nose Geometry on Slender-Body Supersonic Aerodynamics," *Journal of Spacecraft and Rockets*, Vol. 25, No. 2, 1988, pp. 189–193.

[4]Carlson, H. W., and Gapcynski, J. P., "An Experimental Investigation At a Mach Number of 2.01 of the Effects of Body Cross-Section Shape on the Aerodynamic Characteristics of Bodies and Wing-Body Combinations," NACA RM L55E23, July 1955.

[5]Jorgensen, L. H., "Inclined Bodies of Various Cross Sections at Supersonic Speeds," NASA Memo. 10-3-58A, Nov. 1958.

[6]Sigal, A., "Methods of Analysis and Experiments for Missiles with Noncircular Fuselages," *Tactical Missile Aerodynamics: Prediction Methodology*, edited by M. R. Mendenhall, Vol. 142, Progress in Aeronautics and Astronautics Series, AIAA, Washington, DC, 1991, pp. 171–224.

[7]Krieger, R. J., and Williams, J. E., "Accuracy Criteria for Evaluating Supersonic Missile Aerodynamic Coefficient Predictions," *Journal of Spacecraft and Rockets*, Vol. 20, No. 4, 1983, pp. 323–330.

[8]Pitts, W. C., Nielsen, J. N., and Kaatari, G. E., "Lift and Center of Pressure of Wing-Body-Tail Combinations at Subsonic, Transonic, and Supersonic Speeds," NASA Rept. 1307, July 1953.

[9]Hemsch, M. J., "Component Build-Up Method for Engineering Analysis of Missiles at Low-to-High Angles of Attack," *Tactical Missile Aerodynamics: Prediction Methodology*, edited by M. R. Mendenhall, Vol. 142, Progress in Aeronautics and Astronautics Series, AIAA, Washington, DC, 1991, pp. 115–169.

[10]Hemsch, M. J., and Nielsen, J. N., "Equivalent Angle of Attack Method for Estimating the Nonlinear Aerodynamics of Missile Fins," *Journal of Spacecraft and Rockets*, Vol. 20, No. 4, 1983, pp. 356–362.

[11]Hemsch, M. J., Nielsen, J. N., Smith, C. A., and Perkins, S. C., Jr., "Component Aerodynamic Characteristics of Banked Cruciform Missiles With Arbitrary Control Deflections," AIAA Paper 77-1153, Aug. 1977.

[12]Vukelich, S. R., and Jenkins, J. E., "Evaluation of Component Buildup Methods for Missile Aerodynamics Predictions," *Journal of Spacecraft and Rockets*, Vol. 19, No. 6, 1983, pp. 481–488.

[13]Stoy, S. L., and Vukelich, S. R., "Prediction of Aerodynamic Characteristics of Unconventional Missile Configurations Using Component Buildup Technique," AIAA Paper 86-0489, Jan. 1986.

[14]Stoy, S. L., and Vukelich, S. R., "Extension of the Equivalent Angle of Attack Prediction Method," AIAA Paper 84-0311, Jan. 1984.

[15]Nielson, J. N., *Missile Aerodynamics*, McGraw–Hill, New York, 1960, pp. 21, 112–120, 213–219; republished by Nielsen Engineering and Research, Mountain View, CA 1988.

[16]Priolo, F. J., and Wardlaw, A. B., Jr., "Supersonic Non-Circular Missile Computations," *Journal of Spacecraft and Rockets*, Vol. 26, No. 3, 1989, pp. 151–157.

[17]Nelson, H. F., "Wing-Body Interference Lift for Supersonic Missiles with Elliptic Cross-Section Fuselages," *Journal of Spacecraft and Rockets*, Vol. 26, No. 5, 1989, pp. 322–329.

[18]Est, B. E., and Nelson, H. F., "Aerodynamic Forces on Noncircular Cross Section Missile Forebodies," *Journal of Aircraft*, Vol. 29, No. 4, 1992, pp. 612–618.

[19]Wardlaw, A. B., Jr., and Davis, S. F., "A Second Order Godunov Method for Tactical Missiles," Naval Surface Weapons Center. NSWC-TR 86-506, Silver Spring, MD, Dec. 1986.

[20]Wardlaw, A. B., Jr., and Priolo, F. J., "Applying the ZEUS Code," Naval Surface Weapons Center, NSWC-TR 86-508, Silver Spring, MD, Dec. 1986.

[21]Wardlaw, A. B., Jr., Priolo, F. J., and Solomon, J. M., "Multiple-Zone Strategy for Supersonic Missiles," *Journal of Spacecraft and Rockets*, Vol. 24, No. 4, 1987, pp. 377–384.

[22]Wardlaw, A. B., Jr., Baltakis, F. P., Martin, F. M., Priolo, F. J., and Jettmar, R. U., "A Godunov Method for Supersonic Tactical Missiles," *Journal of Spacecraft and Rockets*, Vol. 24, No. 1, 1987, pp. 40–47.

[23]Glaz, H. M., and Wardlaw, A. B., Jr., "A High-Order Godunov Scheme for Steady Supersonic Gas Dynamics," *Journal of Computational Physics*, Vol. 58, No. 2, 1985, pp. 157–187.

[24]Polhamus, E. C., Geller, E. W., and Grunwald, K. J., "Pressure and Force Characteristics of Noncircular Cylinders as Affected by Reynolds Number With a Method Included for Determining the Potential Flow About Arbitrary Shapes," NASA TR R-46, March 1959.

[25]Jenn, A. A., and Nelson, H. F., "Wing Vertical Position Effects on Lift for Supersonic Delta Wing Missiles," *Journal of Spacecraft and Rockets*, Vol. 26, No. 4, 1989, pp. 210–216.

J. E. Daywitt
Associate Editor